



CHORUS

This is the accepted manuscript made available via CHORUS. The article has been published as:

Disentangling surface and bulk transport in topological-insulator p-n junctions

Dirk Backes, Danhong Huang, Rhodri Mansell, Martin Lanius, Jörn Kampmeier, David Ritchie, Gregor Mussler, Godfrey Gumbs, Detlev Grützmacher, and Vijay Narayan

Phys. Rev. B **96**, 125125 — Published 18 September 2017

DOI: [10.1103/PhysRevB.96.125125](https://doi.org/10.1103/PhysRevB.96.125125)

Disentangling surface and bulk transport in topological insulator p - n junctions

Dirk Backes,^{1,*} Danhong Huang,² Rhodri Mansell,¹ Martin Lanius,³ Jörn Kampmeier,³ David Ritchie,¹ Gregor Mussler,³ Godfrey Gumbs,⁴ Detlev Grützmacher,³ and Vijay Narayan^{1,†}

¹*Cavendish Laboratory, University of Cambridge,
J. J. Thomson Avenue, Cambridge CB3 0HE, United Kingdom*

²*Air Force Research Laboratory, Space Vehicles Directorate,
Kirtland Air Force Base, New Mexico 87117, USA*

³*Peter Grünberg Institute (PGI-9), Forschungszentrum Jülich, 52425 Jülich, Germany*

⁴*Department of Physics and Astronomy, Hunter College of the City University of New York,
695 Park Avenue, New York, New York 10065, USA*

(Dated: August 21, 2017)

By combining n -type Bi_2Te_3 and p -type Sb_2Te_3 topological insulators, vertically stacked p - n junctions can be formed, allowing to position the Fermi level into the bulk band gap and also tune between n - and p -type surface carriers. Here we use low-temperature magnetotransport measurements to probe the surface and bulk transport modes in a range of vertical $\text{Bi}_2\text{Te}_3/\text{Sb}_2\text{Te}_3$ heterostructures with varying relative thicknesses of the top and bottom layers. With increasing thickness of the Sb_2Te_3 layer we observe a change from n - to p -type behavior via a specific thickness where the Hall signal is immeasurable. Assuming that the bulk and surface states contribute in parallel, we can calculate and reproduce the dependence of the Hall and longitudinal components of resistivity on the film thickness. This highlights the role played by the bulk conduction channels which, importantly, cannot be probed using surface sensitive spectroscopic techniques. Our calculations are then buttressed by a semi-classical Boltzmann transport theory which rigorously shows the vanishing of the Hall signal. Our results provide crucial experimental and theoretical insights into the relative roles of the surface and bulk in the vertical topological p - n junctions.

PACS numbers: 73.20.-r, 73.25.+i, 73.50.-h

I. INTRODUCTION

Topological insulators (TIs) are bulk insulators with exotic ‘topological surface states’¹ (TSS) which are robust to backscattering from non-magnetic impurities, exhibit spin-momentum locking² and have a Dirac-like dispersion³⁻⁵. These unique characteristics present several opportunities for applications in spintronics, thermoelectricity, and quantum computation. However, a major drawback of ‘early generation’ TIs such as $\text{Bi}_{1-x}\text{Sb}_x$ ⁵ and Bi_2Se_3 ^{2,3} is that the Fermi level E_F intersects the conduction/valence bands, thus giving rise to finite conductivity in the bulk. This non-topological conduction channel conducts in parallel to the TSS and in turn subverts the overall topological nature. Thus, in order to create bona fide TIs, the Fermi level E_F needs to be tuned within the bulk bandgap, and this has previously been achieved by means of electrical gating⁶⁻⁹, doping^{4,10-12}, or, as recently reported, by creating p - n junctions from two different TI films^{13,14}.

In Ref. 14 a ‘vertical topological p - n junction’ was realized by growing an n -type Bi_2Te_3 layer capped by a layer of p -type Sb_2Te_3 , and it was shown that varying the relative layer thicknesses serves to tune E_F without the use of an external field. Importantly, such bilayer systems are expected to be significantly less disordered than doped materials such as $(\text{Bi}_{1-x}\text{Sb}_x)_2\text{Te}_3$ in which inhomogeneity of the dopants is a constant problem^{12,15}. Furthermore, and in sharp contrast to doped TIs, the intrinsic p and n character of the individual layers presents re-

markable opportunities towards the observation of novel physics including Klein tunneling^{16,17}, spin interference effects at the p - n interface¹⁸, and topological exciton condensates¹⁹. However, currently there exists little understanding of the bulk conduction in such topological p - n junctions, primarily because ARPES used in Ref. 14 is a surface-sensitive method. This is especially noteworthy in light of the fact that the band structure varies along the depth of the TI p - n junction slab, in sharp contrast to the essentially constant band gap within the bulk of $(\text{Bi}_{1-x}\text{Sb}_x)_2\text{Te}_3$ -type compounds. Understanding and minimizing the bulk conduction channels in TI p - n junctions is crucial in order to realize their technological potential as well as to gain access to the exotic physics they can host.

II. EXPERIMENT

$\text{Bi}_2\text{Te}_3/\text{Sb}_2\text{Te}_3$ -bilayers (BST) were grown on phosphorous doped Si substrates using molecular beam epitaxy (MBE). Details of the MBE sample preparation can be found in Ref. 14. In all the samples, the bottom Bi_2Te_3 -layer had thickness $t_{\text{BiTe}} = 6$ nm while the top Sb_2Te_3 -layers had thicknesses $t_{\text{SbTe}} = 6.6$ nm (BST6), 7.5 nm (BST7), 15 nm (BST15), and 25 nm (BST25), respectively. The layers were patterned into Hall bars of width $W = 200$ μm and length $L = 1000$ μm using photoresist as a mask for ion milling, and Ti/Au contact pads were deposited for electrical contact. Low- T electrical

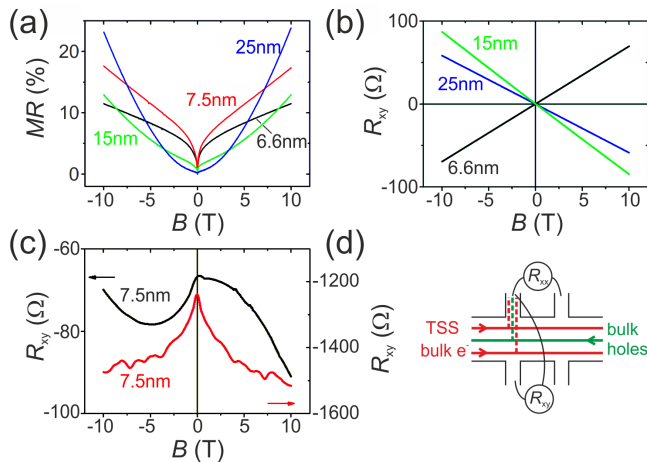


FIG. 1. (a) MR and (b+c) R_{xy} as a function of B for different t_{SbTe} . All curves are measured at 280 mK. The high field MR is linear for thin samples and changes to parabolic for thicker samples. Cusp-like deviations at low fields are due to WAL corrections. The sign change of the slope in (b) indicates transport by electrons for BST6 and by holes for BST15 and BST25. No Hall slope is visible in (c) for 2 different pairs of contacts of BST7. (d) The schematic shows the charge transport channels in a longitudinal and transverse measurement setup. Trajectories of TSS and bulk electrons are shown in red and of bulk holes in green.

69 measurements were carried out using lock-in techniques
 70 in a He-3 cryostat with a base temperature of 280 mK and
 71 a 10 T superconducting magnet. Both longitudinal (R_{xx})
 72 and transverse (R_{xy}) components of resistance were measured.
 73

74 III. RESULTS

75 Figure 1(a) shows the longitudinal magnetoresistance
 76 ($\text{MR} \equiv (R_{xx}(B) - R_{xx}(0))/R_{xx}(0)$) of the various sam-
 77 ples considered. We find that above ~ 2 T the MR in
 78 BST6 and BST7 is manifestly linear whereas the MR in
 79 BST15 and BST25 appears to be neither purely linear nor
 80 quadratic. While there is experimental evidence suggest-
 81 ing an association between linear MR and linearly disper-
 82 sive media^{20–22}, as well as a theoretical basis for this asso-
 83 ciation²³, we note that disorder can also render giant lin-
 84 ear MR^{24,25} by admixing longitudinal and Hall voltages.
 85 In Fig. 1(b) we see that R_{xy} is linear in B and its slope
 86 changes sign from positive (BST6) to negative (BST15
 87 and BST25). This is simply a reflection of different
 88 charge carrier types of Bi_2Te_3 (n -type) and Sb_2Te_3 (p -
 89 type), where electrons (holes) dominate transport when
 90 Sb_2Te_3 is thin (thick). Intriguingly, Fig. 1(c) shows R_{xy}
 91 vs B measured in two different Hall bar devices of BST7
 92 to be strongly non-linear and non-monotonic. Qualita-
 93 tively, it appears as if R_{xy} is picking up a large com-
 94 ponent of R_{xx} despite the Hall probes being aligned to
 95 each other with lithographic (μm -scale) precision. We

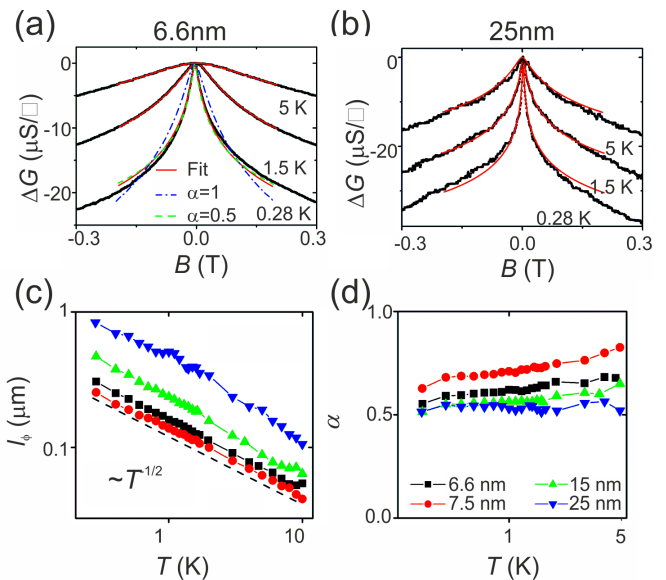


FIG. 2. (a+b) Weak antilocalization peaks for 2 different
 Sb_2Te_3 -thicknesses and at 3 different temperatures. Fits to
 the measurements, based on the HLN model, are shown in
 straight red lines, while curves with α at 0.5 (green dashed
 line) and 1 (blue dashed-dotted line) allow to estimate the
 error. (c) l_ϕ as a function of T for various t_{SbTe} in a log-log
 plot. All curves are proportional to $\propto T^{-0.5}$ (dashed line)
 but shifted with respect to each other. (d) α as a function of T
 for various t_{SbTe} .

96 conjecture, therefore, that BST7 is very close to where
 97 the Hall coefficient R_H precisely changes from positive
 98 to negative. Seemingly to the contrary, ARPES mea-
 99 surements in Ref. 14 reveal that E_F intersects the Dirac
 100 point in samples with $15 \text{ nm} < t_{\text{SbTe}} < 25 \text{ nm}$, in which
 101 parameter regime Fig. 1(b) indicates a net excess of p -
 102 type carriers. The investigation of this discrepancy is the
 103 major focus of this manuscript.

104 Figures 2(a+b) show the low-field MR where a pro-
 105 nounced ‘weak anti-localisation’ (WAL) cusp is visible at
 106 zero magnetic field (B). The WAL corrections are well-
 107 described by the model of Hikami, Larkin and Nagaoka
 108 (HLN)²⁶

$$\begin{aligned} \Delta\sigma_{xx}^{2D} &\equiv \sigma_{xx}^{2D}(B) - \sigma_{xx}^{2D}(0) \\ &= \alpha \frac{e^2}{2\pi^2\hbar} \left[\ln \left(\frac{\hbar}{4eBl_\phi^2} \right) - \psi \left(\frac{1}{2} + \frac{\hbar}{4eBl_\phi^2} \right) \right]. \end{aligned} \quad (1)$$

109 Here $\sigma_{xx} \equiv (L/W)R_{xx}/(R_{xx}^2 + R_{xy}^2)$ and the super-
 110 script 2D indicates that the equation is valid for a two-
 111 dimensional conducting sheet, α is a parameter = 0.5 for
 112 each 2D WAL channel, e is the electronic charge, \hbar is
 113 Planck’s constant divided by 2π , l_ϕ is the phase coher-
 114 ence length, and ψ is the digamma function.

115 Figure 2(c) shows the T -dependence of l_ϕ for all sam-
 116 ples. We find that $l_\phi \propto T^{-p/2}$, where the exponent $p = 1$
 117 is in line with 2D Nyquist scattering^{27,28} due to electron-

118 electron scattering processes. The second fitting param-
 119 eter α is depicted in Fig. 2(d) and we find values consis-
 120 tent with $\alpha = 0.5$ (error estimates on α can be found in
 121 Fig. 2(a) and a discussion in Appendix A). This is consis-
 122 tent with several previous reports on TI thin films^{9,29–31}.

123 IV. DISCUSSION

124 A. 3-channel model

125 Having ascertained that the transport characteristics
 126 of the $\text{Bi}_2\text{Te}_3/\text{Sb}_2\text{Te}_3$ heterostructures are consistent
 127 with conventional TI behaviour, we now proceed to un-
 128 derstand the Hall characteristics. It is well-known that
 129 the TIs Bi_2Te_3 and Sb_2Te_3 show bulk conduction in ad-
 130 dition to the TSS. Thus, we start with a simple picture
 131 of three independent conduction channels: bulk n - and
 132 p -type layers corresponding to the Bi_2Te_3 and Sb_2Te_3
 133 layers, respectively, and a TSS on the top surface. While
 134 in principle a TSS exists also at the interface with the
 135 substrate, it is expected that its contribution to the con-
 136 ductivity is largely diminished due to the strongly disor-
 137 dered TI-substrate interface^{31,32}. Thus as a first approx-
 138 imation, we do not consider the bottom TSS.

139 Our starting point is the expressions for σ_{xx} and R_H
 140 in a multi-channel system^{33–35}

$$\sigma_{xx} = e n_p \mu_p - e n_n \mu_n \pm e n_t \mu_t \quad (2)$$

$$R_H(t_{\text{SbTe}}) \equiv \frac{1}{e \cdot n_{\text{eff}}} = \frac{n_p \mu_p^2 - n_n \mu_n^2 \pm n_t (t_{\text{SbTe}}) \mu_t^2}{e(n_p \mu_p + n_n \mu_n + n_t (t_{\text{SbTe}}) \mu_t)} \quad (3)$$

141 Here n_{eff} is the effective carrier concentration, e is the
 142 charge of an electron and $-e$ is the charge of a hole, the
 143 subscript n , p and t signify bulk electrons, bulk holes, and
 144 surface carriers, respectively, n_i are carrier concentra-
 145 tions, and μ_i represent the mobility of the charge carriers.
 146 The \pm indicates, respectively, negative ($t_{\text{SbTe}} < 20$ nm)
 147 and positive charge carriers ($t_{\text{SbTe}} > 20$ nm) in the TSS.
 148 The following literature values for the bulk layers are as-
 149 sumed: $n_{\text{BiTe}} = 8 \times 10^{19} \text{ cm}^{-3}$ and $\mu_n = 50 \text{ cm}^2 \text{ V}^{-1} \text{ s}^{-1}$
 150 for Bi_2Te_3 ¹² and $n_{\text{SbTe}} = 4.5 \times 10^{19} \text{ cm}^{-3}$ and $\mu_p =$
 151 $300 \text{ cm}^2 \text{ V}^{-1} \text{ s}^{-1}$ for Sb_2Te_3 ^{12,28,36}. In order to compare
 152 n_{BiTe} and n_{SbTe} to the TSS carrier concentration, we con-
 153 vert them to effective areal densities as $n_n \equiv n_{\text{BiTe}} \cdot t_{\text{BiTe}}$
 154 and $n_p \equiv n_{\text{SbTe}} \cdot t_{\text{SbTe}}$. It can be shown that $n_t \propto E_B^2$
 155 where E_B is the difference between E_F and Dirac point
 156 (see Eq. B3, Appendix B) and E_B , in turn, can be re-
 157 trieved from ARPES measurements in Ref.¹⁴. μ_t is used
 158 as a fitting parameter.

159 Figure 3(a) shows R_H as predicted by the model us-
 160 ing the above parameters to be in good agreement with
 161 the measured values. However, for the same parame-
 162 ters we find that $R_{xx} \equiv (L/W)\sigma_{xx}$ is significantly under-
 163 estimated especially for low t_{SbTe} (Fig. 3(b)). A likely

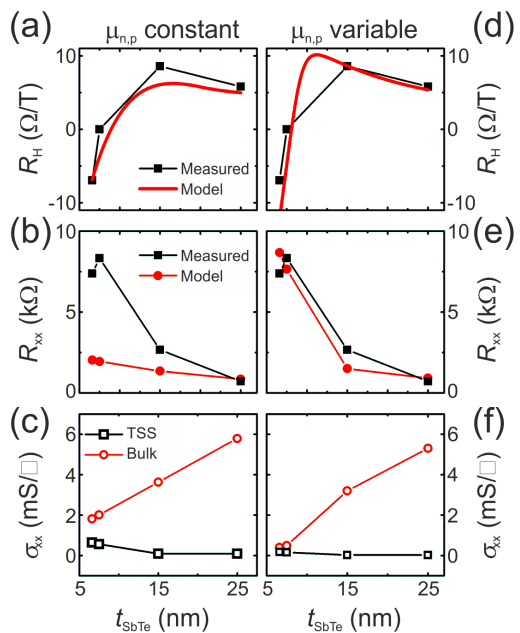


FIG. 3. (a+d) Hall slopes R_H determined from the Hall measurements in Fig. 1(b) (black square), and fitted using Eq. 3 (red lines). The bulk mobilities $\mu_{n,p}$ were kept constant in (a) and reduced for low thicknesses in (d). (b+c) Comparison of measured (black squares) and calculated total resistance (red disks), and conductivity of the TSS (black open squares) and of the bulk (red open disks), using fitting parameters from (a). (e+f) Same as (b+c) but using fitting parameter from (d). All variables are a function of t_{SbTe} .

164 source of this discrepancy is that the bulk μ_i values are
 165 not applicable for the ultra-thin films. This is especially
 166 so considering the fact that a depletion zone will form
 167 at the p - n interface. Determining the exact profile of
 168 the charge carrier density at the interface is beyond the
 169 scope of this paper and instead, we demonstrate that an
 170 *ad-hoc* thickness-dependent reduction of μ_i of the *bulk*
 171 layers with all other parameters unchanged, can signifi-
 172 cantly improve the quality of the predictions. Figure 3(d)
 173 shows the result of a fit in which μ_p and μ_n are reduced to
 174 20% of their bulk value in BST6 and BST7, and to 95%
 175 of their bulk value in BST15 and BST25. Not only do we
 176 obtain excellent agreement with the R_H data, the model
 177 is also able to accurately predict R_{xx} (Fig. 3(e)). The ob-
 178 tained value of $\mu_t = 281 \pm 17 \text{ cm}^2 \text{ V}^{-1} \text{ s}^{-1}$ is well within
 179 the range of previous studies in ultra-thin TIs where the
 180 TSS dominate transport¹¹.

181 Figure 3(f) shows the important physical insight we ar-
 182 rive at on the basis of this simple model: the bulk contribu-
 183 tion is drastically reduced in thin films (see Fig. 3(c)),
 184 with the TSS eventually dominating the overall conduc-
 185 tivity σ_{tot} (see Fig. 3(f)).

186 To test this conclusion we measure samples with top-
 187 gate electrodes which enable the tuning of the Fermi level
 188 E_F via a gate voltage V_G . A variation of E_F should
 189 lead to perceptible changes of the transport properties

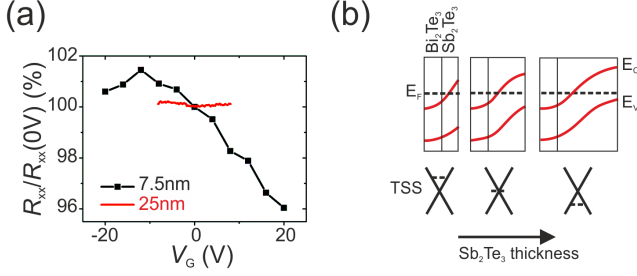


FIG. 4. (a) Gate voltage dependence of the resistivity for BST7 (black) and BST25 (red). (b) Schematic of the change of band structure as $t_{\text{Sb}_2\text{Te}_3}$ is increased.

of the TSS (see Fig. 4(b)) while transport through the bulk should be less affected due to screening. As can be seen in Fig. 4(a) this is indeed the case, with the resistance of the thin, TSS dominated sample much more dependent on V_G than the thick, bulk dominated sample. The resistance of the thin sample is maximized when $V_G = -12\text{ V}$, likely corresponding to the alignment of E_F with the Dirac point. Thus, broadly speaking, despite the basic nature of the model, it captures the essential physics and provides a consistent explanation of the dependence of the longitudinal and Hall transport components. Furthermore, the results of our calculation are

$$\mathbf{j}_{c,v}^{\parallel}(z) = \frac{2e\gamma_{e,h}m_{e,h}^*\tau_{e,h}(z)}{\tau_{p(e,h)}(z)} \mathbf{v}_{c,v}^{\parallel}[u_{c,v}(z)] \left\{ \left[\overleftrightarrow{\boldsymbol{\mu}}_{c,v}^{\parallel}(\mathbf{B}, z) \cdot \mathbf{E} \right] \right\} \cdot \mathbf{v}_{c,v}^{\parallel}[u_{c,v}(z)] \mathcal{D}_{c,v}[u_{c,v}(z)], \quad (4)$$

where $\gamma_{e,h} = -1$ or $+1$ for electrons and holes, respectively, $m_{e,h}^*$ are effective masses of electrons and holes, $\tau_{e,h}(z)$ and $\tau_{p(e,h)}(z)$ are bulk energy- and momentum relaxation times³⁷, the velocity $\mathbf{v}_{c,v}^{\parallel}(\mathbf{k}) = -\gamma_{e,h} \hbar \mathbf{k}_{\parallel} / m_{e,h}^*$ (with \mathbf{k} the wavevector and \mathbf{k}_{\parallel} the in-plane wavevector), $u_{c,v}(z) = (\hbar k_F^{e,h})^2 / 2m_{e,h}^*$ and $k_F^{e,h}$ are Fermi energies and wave vectors in the bulk, $\overleftrightarrow{\boldsymbol{\mu}}_{c,v}^{\parallel}$ are mobility tensors, and $\mathcal{D}_{c,v}[u_{c,v}(z)] = (\sqrt{u_{c,v}(z)} / 4\pi^2) (2m_{e,h}^* / \hbar^2)^{3/2}$ is the electron and hole density-of-states per spin.

Similarly, one obtains the surface current per length as

$$\mathbf{j}_s^{\pm} = \mp \frac{e\tau_s \hbar k_F^s}{\tau_{sp} v_F} \mathbf{v}_s^{\pm}(u_s) \left\{ \left[\overleftrightarrow{\boldsymbol{\mu}}_s^{\pm}(\mathbf{B}) \cdot \mathbf{E} \right] \right\} \cdot \mathbf{v}_s^{\pm}(u_s) \rho_s(u_s), \quad (5)$$

where the \pm denote when the Fermi level lies above and below the Dirac point, respectively, τ_s and τ_{sp} are surface energy- and momentum relaxation times, $k_F^s = \sqrt{4\pi n_s}$ where n_s is the areal density of surface electrons, v_F is the Fermi velocity of a Dirac cone, $\mathbf{v}_s^{\pm}(\mathbf{k}_{\parallel}) = \pm(\mathbf{k}_{\parallel} / k_{\parallel}) v_F$, $u_s = \hbar v_F k_F^s$ is the Fermi energy of a Dirac cone, and $\rho_s(u_s) = u_s / (2\pi \hbar^2 v_F^2)$ is the surface density-of-states of a

clearly consistent with the observation of ‘no’ Hall slope in BST7.

B. Semi-classical theory

Although our simplistic model offers useful physical insights, for a more microscopic understanding it is desirable that one is not dependent on *ad-hoc* assumptions and/or a large number of experimental parameters. In the following we present a semi-classical theory for calculating magneto-conductivity tensors of surface and bulk charge carriers in a topological p - n junction using zeroth and first-order Boltzmann moment equations³⁷. Assuming the p - n interface to be in the x - y plane, then under a parallel external electric field $\mathbf{E} = (E_x, E_y, 0)$ and a perpendicular magnetic field $\mathbf{B} = (0, 0, B)$, the total current per length in a p - n junction structure is given by $\int_{-L_A}^{L_D} dz \left[\mathbf{j}_c^{\parallel}(z) + \mathbf{j}_v^{\parallel}(z) \right] + \mathbf{j}_s^{\pm}$, where L_D and L_A are the thickness of the p region (donors) and n region (acceptors), respectively. Here \mathbf{j}_i indicate the current densities with $i = c, v$ or s for conduction band, valence band and surface, respectively. The superscript \parallel is included to emphasise that the current considered is parallel to the p - n interface as is experimentally the case. The bulk current densities are given by

Dirac cone.

The bulk mobility tensors $\overleftrightarrow{\boldsymbol{\mu}}_{c,v}^{\parallel}(\mathbf{B}, z)$ are given by

$$\overleftrightarrow{\boldsymbol{\mu}}_{c,v}^{\parallel}(\mathbf{B}, z) = \frac{\mu_0(z)}{1 + \mu_0^2(z)B^2} \begin{bmatrix} 1 & \mu_0(z)B \\ -\mu_0(z)B & 1 \end{bmatrix}, \quad (6)$$

where $\mu_0(z) = e\gamma_{e,h}\tau_{p(e,h)}(z) / m_{e,h}^*$. A derivation of the bulk mobility tensor can be found in Appendix D. The bulk conductivity tensor is then calculated as

$$\overleftrightarrow{\boldsymbol{\sigma}}_{c,v}^{\parallel}(\mathbf{B}) = e\gamma_{e,h} \int_{-L_A}^{L_D} dz n_{e,h}(z) \left[\frac{\tau_{e,h}(z)}{\tau_{p(e,h)}(z)} \right] \overleftrightarrow{\boldsymbol{\mu}}_{c,v}^{\parallel}(\mathbf{B}, z). \quad (7)$$

Likewise, the surface mobility tensor is

$$\overleftrightarrow{\boldsymbol{\mu}}_s^{\pm}(\mathbf{B}) = \mp \frac{\mu_1}{1 + \mu_1^2 B^2} \begin{bmatrix} 1 & \mp \mu_1 B \\ \pm \mu_1 B & 1 \end{bmatrix}, \quad (8)$$

where $\mu_1 = 4e_0^2 \epsilon_r^2 \hbar v_F^2 / \sigma_i e^3$, ϵ_r is the host dielectric constant, and σ_i is the surface density of impurities. This corresponds to a surface conductivity tensor given by

$$\hat{\sigma}_s^\pm(\mathbf{B}) = e\sigma_s \left(\frac{\tau_s}{\tau_{sp}} \right) \hat{\mu}_s^\pm(\mathbf{B}). \quad (9)$$

$$\begin{aligned} \hat{\sigma}_{\text{tot}}(\mathbf{B}) &= e \hat{\mu}_v^\parallel(\mathbf{B}) N_A A_h \left[(L_A - W_p) + \int_0^{W_p} dz \exp\left(-\frac{\beta e \bar{\mu}_h N_A}{2\epsilon_0 \epsilon_r D_h} z^2\right) \right] - e \hat{\mu}_c^\parallel(\mathbf{B}) N_D A_e \\ &\times \left[(L_D - W_n) + \int_0^{W_n} dz \exp\left(-\frac{\beta e \bar{\mu}_e N_D}{2\epsilon_0 \epsilon_r D_e} z^2\right) \right] + e \hat{\mu}_s^\pm(\mathbf{B}) \left(\frac{\alpha_0^2}{4\pi \hbar^2 v_F^2} \right) (L_A - L)^2 A_s, \end{aligned} \quad (10)$$

where α_0 and L_0 are constants to be determined experimentally, $N_{D,A}$ are doping concentrations, W_n and W_p are the thicknesses of the depletion zones for donors and acceptors in a p - n junction, $\bar{\mu}_{e,h}$ are $\mu_0(z)$ evaluated at $n_{e,h}(z) = N_{D,A}$, $D_{e,h}$ are diffusion coefficients, $\beta = 4/3$ ($\beta = 7/3$) for longitudinal (Hall) conductivity. In addition, the averaged mobilities $\hat{\mu}_{c,v}^\parallel(\mathbf{B})$ are defined by their values of $\tau_{p(e,h)}(z)$ at $n_{e,h}(z) = N_{D,A}$, and three coefficients are $A_s = \tau_s/\tau_{sp} \approx 3/4$,

$$\begin{aligned} A_{e,h} &= \frac{\tau_{e,h}(z)}{\tau_{p(e,h)}(z)} \Big|_{n_{e,h}(z)=N_{D,A}} \\ &= \frac{1}{6} \left(\frac{Q_c}{k_{F,e,h}^e} \right)^2 \left[2 \ln \left(\frac{2k_{F,e,h}^e}{Q_c} \right) - 1 \right] \\ &= \frac{Q_c^2}{6(3\pi^2 N_{D,A})^{2/3}} \left\{ 2 \ln \left[\frac{2(3\pi^2 N_{D,A})^{1/3}}{Q_c} \right] - 1 \right\}, \end{aligned} \quad (11)$$

where $1/Q_c$ is the Thomas-Fermi screening length. More details on the derivation of the conductivity tensors can be found in Appendix E.

From Eq. 10 one can see that there exists a critical value of $L_A = L^*$ at which the total Hall conductivity becomes zero, which is determined from the following quadratic equation

$$\begin{aligned} &\frac{\bar{\mu}_h^2 N_A A_h}{1 + \bar{\mu}_h^2 B^2} \left\{ (L^* - W_p) + \int_0^{W_p} dz \exp\left[-\left(\frac{7e\bar{\mu}_h N_A}{6\epsilon_0 \epsilon_r D_h}\right) z^2\right] \right\} - \frac{\bar{\mu}_e^2 N_D A_e}{1 + \bar{\mu}_e^2 B^2} \left\{ (L_D - W_n) \right. \\ &\left. + \int_0^{W_n} dz \exp\left[-\left(\frac{7e\bar{\mu}_e N_D}{6\epsilon_0 \epsilon_r D_e}\right) z^2\right] \right\} \pm \frac{\mu_1^2}{1 + \mu_1^2 B^2} \left(\frac{\alpha_0^2}{4\pi \hbar^2 v_F^2} \right) (L^* - L_0)^2 A_s = 0, \end{aligned} \quad (12)$$

where the sign $+$ ($-$) corresponds to $L_A > L_0$ ($L_A < L_0$) for the contribution of the lower (upper) Dirac cone.

We note that in arriving at the above equations we have not considered scattering between the TSS and bulk layers. Including these will modify energy-relaxation times for both bulk and surface states, although no analytical expression for these can be obtained even at low T . We leave a numerical evaluation of the problem for a later manuscript. For the purposes of this manuscript, we stress that the inclusion of this coupling only serves to modify the three coefficients A_e , A_h , and A_s , and thus the obtained result is qualitatively unchanged. Importantly, the physical content of Eq. 12 is essentially identical to that in Eq. 3, but arrived at in a more rigorous fashion. This provides a very useful microscopic ground-

ing to Eq. 3 whilst also providing additional confidence to the physical insights drawn from the simple three-channel model.

V. CONCLUSION

In conclusion, we have reported low- T magnetotransport measurements on vertical topological p - n junctions and understood the data within a three-channel model for the Hall resistance. It provides useful insights into the complex interplay of the bulk and TSS in the multi-layered TI, explains the sign change of R_H with varying t_{SbTe} , and delivers values for the mobility of the TSS of $281 \text{ cm}^2 \text{ V}^{-1} \text{ s}^{-1}$. We then develop a Boltzmann trans-

port theory which provides a clear microscopic foundation for our model. Our work paves the way for the study of other complex TI heterostructures^{29,38,39}, where bulk states and TSS of different carrier types coexist. In future, our method can be applied to improved topological p - n junctions in which a top and bottom TSS can form novel Dirac fermion excitonic states.

ACKNOWLEDGMENTS

D.B., D.R. and V.N. acknowledge funding from the Leverhulme Trust, UK, D.B., R.M., D.R., and V.N. acknowledge funding from EPSRC (UK). DH would like to thank the support from the Air Force Office of Scientific Research (AFOSR). G.M., M.L., J.K. and D.G. acknowledge financial support from the DFG-funded priority programme SPP1666.

Appendix A: Error estimates for α

Figure 2(a) compares the results when 1) α and l_ϕ were both fitting variables (red line) or 2) when l_ϕ alone was used as a fitting variable and α was kept constant. We find that the fit for $\alpha = 1$ (blue dashed-dotted line) is of a significantly poorer quality, indicating clearly that the data is consistent with the existence of one WAL mode. This errors become significantly larger as T is increased (here not shown) and thus one must not over interpret the apparent increase in α with T in Fig. 2(d).

Appendix B: TSS electron density

The density of states in the dirac cone³³ is given by

$$g(k)dk/\frac{2\pi^2}{L} = 2\pi kdk/\frac{2\pi^2}{L} = \frac{kdk}{(2\pi/L)^2} \quad (\text{B1})$$

The relation between the binding energy E_B , i.e. the difference between the Fermi energy and the Dirac point, and the Fermi wave vector k_F is

$$E_B = \beta k_F = \hbar v_F k_F \quad (\text{B2})$$

and can be retrieved from ARPES measurements in Ref. 14, carried out using samples from the same growth process and identical material parameters. For $E_B = 215$ meV, $k_F \approx 0.1\text{\AA}$ (see Fig. 4(h) in Ref. 14), thus $\beta = \frac{E_B}{k_F} = 3.44 \cdot 10^{-29}$ J m. From β , a Fermi velocity of $3.26 \cdot 10^5 \frac{\text{m}}{\text{s}}$ can be derived.

The electron density of the TSS is

$$n_t = k_F^2/4\pi = \frac{E_B^2}{4\pi\beta^2} \quad (\text{B3})$$

Furthermore, the relation between E_B and the Sb_2Te_3 -thickness is linear ($dE_B/dt_{\text{SbTe}} = 1.62 \cdot 10^{-12}$ J/m, see Fig. 5) and

$$n_t = \frac{(dE_B/dt_{\text{SbTe}} \cdot t_{\text{SbTe}})^2}{4\pi\beta^2} \quad (\text{B4})$$

Appendix C: Derivation of R_H and n_{eff}

The force acting on charges in the TSS (index t), bulk- Sb_2Te_3 (p) and bulk- Bi_2Te_3 (n) originate from an electric field \vec{E} in y -direction and a magnetic field \vec{B} in z -direction:

$$\begin{aligned} -F_{ny} &= eE_y + ev_{nx}B_z \\ -F_{ty} &= eE_y + ev_{tx}B_z \\ F_{py} &= eE_y - ev_{px}B_z \end{aligned} \quad (\text{C1})$$

Using $v = \frac{\mu}{e}F$ with μ the mobility, we obtain

$$\begin{aligned} \frac{v_{ny}}{\mu_n} &= E_y + \mu_n E_x B_z \\ \frac{v_{ty}}{\mu_t} &= E_y + \mu_t E_x B_z \\ \frac{v_{py}}{\mu_p} &= E_y - \mu_p E_x B_z \end{aligned} \quad (\text{C2})$$

Furthermore, no charge current is flowing in y -direction

$$\begin{aligned} J_y &= J_n + J_t + J_p \\ &= en_n v_{ny} + en_t v_{ty} + en_p v_{py} = 0 \\ \implies n_n v_{ny} &= -(n_t v_{ty} + n_p v_{py}) \end{aligned} \quad (\text{C3})$$

Inserting the velocities in the previous equation gives

$$\begin{aligned} &n_n \mu_n (E_y + \mu_n E_x B_z) \\ &= -(n_t \mu_t (E_y + \mu_t E_x B_z) + n_p \mu_p (E_y - \mu_p E_x B_z)) \\ \implies E_y (n_n \mu_n + n_t \mu_t + n_p \mu_p) \\ &= B_z E_x (-n_n \mu_n^2 - n_t \mu_t^2 + n_p \mu_p^2) \end{aligned} \quad (\text{C4})$$

The charge current in x -direction is

$$\begin{aligned} J_x &= en_n v_{nx} + en_t v_{tx} + en_p v_{px} \\ &= (n_n \mu_n + n_t \mu_t + n_p \mu_p) e E_x \end{aligned} \quad (\text{C5})$$

E_x can now be replaced, resulting in

$$\begin{aligned} &e E_y (n_n \mu_n + n_t \mu_t + n_p \mu_p)^2 \\ &= B_z J_x (-n_n \mu_n^2 - n_t \mu_t^2 + n_p \mu_p^2) \\ \implies R_H &= \frac{B_z J_x}{E_y} = \frac{-n_n \mu_n^2 - n_t \mu_t^2 + n_p \mu_p^2}{e(n_n \mu_n + n_t \mu_t + n_p \mu_p)^2} \end{aligned} \quad (\text{C6})$$

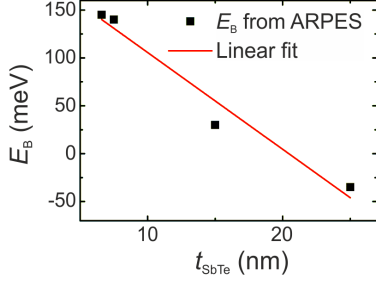


FIG. 5. Relation between E_B and t_{SbTe} (from Ref. 14)

Both n_p and n_t are depending on the thickness of the Sb_2Te_3 -thickness, t_{SbTe} , with

$$n_p = n_{\text{SbTe}} \cdot t_{\text{SbTe}}$$

$$n_t(t_{\text{SbTe}}) = \frac{(dE_B/dt_{\text{SbTe}} \cdot (t_{\text{SbTe}} - t_0))^2}{4\pi\beta^2} \quad (\text{C7})$$

where dE_B/dt_{SbTe} can be gained from Fig. 5.

Thus $R_H(t_{\text{SbTe}})$ is a function of the Sb_2Te_3 -thickness of the form

$$R_H(t_{\text{SbTe}}) = \frac{-n_n(t_{\text{SbTe}})\mu_n^2 \pm n_t(t_{\text{SbTe}})\mu_t^2 + n_p\mu_p^2}{e(n_n(t_{\text{SbTe}})\mu_n + n_t(t_{\text{SbTe}})\mu_t + n_p\mu_p)^2}$$

$$= \frac{-n_{\text{SbTe}}t_{\text{SbTe}}\mu_n^2 \pm \frac{(dE_B/dt_{\text{SbTe}} \cdot (t_{\text{SbTe}} - t_0))^2}{4\pi\beta^2} \mu_t^2 + n_p\mu_p^2}{e(n_{\text{SbTe}}t_{\text{SbTe}}\mu_n + \frac{(dE_B/dt_{\text{SbTe}} \cdot (t_{\text{SbTe}} - t_0))^2}{4\pi\beta^2} \mu_t + n_p\mu_p)^2} \quad (\text{C8})$$

where the '+' sign has to be used when $t_{\text{SbTe}} > 20$ nm and the '-' sign for $t_{\text{SbTe}} < 20$ nm.

Because of the entity $R_H = -1/(e \cdot n_{\text{eff}})$, the 'effective' 2-dimensional charge density is given by

$$n_{\text{eff}} = -\frac{(n_n(t_{\text{SbTe}})\mu_n + n_t(t_{\text{SbTe}})\mu_t + n_p\mu_p)^2}{-n_n(t_{\text{SbTe}})\mu_n^2 \pm n_t(t_{\text{SbTe}})\mu_t^2 + n_p\mu_p^2} \quad (\text{C9})$$

$$\vec{\mathcal{C}} = \begin{bmatrix} 1 + q\tau_1(r_{12}B_3 - r_{13}B_2) & q\tau_1(r_{13}B_1 - r_{11}B_3) & q\tau_1(r_{11}B_2 - r_{12}B_1) \\ q\tau_2(r_{22}B_3 - r_{23}B_2) & 1 + q\tau_2(r_{23}B_1 - r_{21}B_3) & q\tau_2(r_{21}B_2 - r_{22}B_1) \\ q\tau_3(r_{32}B_3 - r_{33}B_2) & q\tau_3(r_{33}B_1 - r_{31}B_3) & 1 + q\tau_3(r_{31}B_2 - r_{32}B_1) \end{bmatrix}, \quad (\text{D4})$$

as well as the source vector \mathbf{s} , given by

$$\mathbf{s} = \begin{bmatrix} q\tau_1(r_{11}E_1 + r_{12}E_2 + r_{13}E_3) \\ q\tau_2(r_{21}E_1 + r_{22}E_2 + r_{23}E_3) \\ q\tau_3(r_{31}E_1 + r_{32}E_2 + r_{33}E_3) \end{bmatrix}, \quad (\text{D5})$$

we can reduce the linear equations to a matrix equation

$\vec{\mathcal{C}} \cdot \mathbf{v}_d = \mathbf{s}$ with a formal solution $\mathbf{v}_d = \vec{\mathcal{C}}^{-1} \cdot \mathbf{s}$. Explicitly,

Appendix D: Bulk and surface mobility tensors

By using the force-balance equation^{37,40,41} for bulk electrons

$$\frac{\partial \mathbf{v}_d(t|z)}{\partial t} = -\vec{\tau}_{pe}^{-1}(z) \cdot \mathbf{v}_d(t|z)$$

$$- e\vec{\mathcal{M}}_c^{-1}(z) \cdot [\mathbf{E}(t) + \mathbf{v}_d(t|z) \times \mathbf{B}(t)] = 0, \quad (\text{D1})$$

as well as the diagonal approximation for the inverse momentum-relaxation-time tensor $\vec{\tau}_{pe}^{-1} \approx (1/\tau_j) \delta_{ij}$, we get the following group of linear inhomogeneous equations for $\mathbf{v}_d = \{v_1, v_2, v_3\}$

$$[1 + q\tau_1(r_{12}B_3 - r_{13}B_2)]v_1 + q\tau_1(r_{13}B_1 - r_{11}B_3)v_2 + q\tau_1(r_{11}B_2 - r_{12}B_1)v_3 = q\tau_1(r_{11}E_1 + r_{12}E_2 + r_{13}E_3),$$

$$q\tau_2(r_{22}B_3 - r_{23}B_2)v_1 + [1 + q\tau_2(r_{23}B_1 - r_{21}B_3)]v_2 + q\tau_2(r_{21}B_2 - r_{22}B_1)v_3 = q\tau_2(r_{21}E_1 + r_{22}E_2 + r_{23}E_3),$$

$$q\tau_3(r_{32}B_3 - r_{33}B_2)v_1 + q\tau_3(r_{33}B_1 - r_{31}B_3)v_2 + [1 + q\tau_3(r_{31}B_2 - r_{32}B_1)]v_3 = q\tau_3(r_{31}E_1 + r_{32}E_2 + r_{33}E_3), \quad (\text{D2})$$

where the statistically-averaged inverse effective-mass tensor for the conduction band is

$$[\vec{\mathcal{M}}_c^{-1}(z)]_{ij} \equiv \{r_{ij}\} \equiv \frac{2}{n_e(z)V} \sum_{\mathbf{k}} \left[\frac{1}{\hbar^2} \frac{\partial^2 \varepsilon_c(\mathbf{k})}{\partial k_i \partial k_j} \right] f_0[\varepsilon_c(\mathbf{k}), T; u_c(z)], \quad (\text{D3})$$

$i, j = x, y, z$, $\mathbf{B} = \{B_1, B_2, B_3\}$, $\mathbf{E} = \{E_1, E_2, E_3\}$, and $q = -e$. By defining the coefficient matrix $\vec{\mathcal{C}}$ for the above linear equations, i.e.,

we find the solution $\mathbf{v}_d = \{v_1, v_2, v_3\}$ for $j = 1, 2, 3$ as

$$v_j = \frac{\text{Det}\{\vec{\Delta}_j\}}{\text{Det}\{\vec{\mathcal{C}}\}}, \quad (\text{D6})$$

where $\text{Det}\{\dots\}$ means taking the determinant,

$$\begin{aligned}
\overleftrightarrow{\Delta}_1 &= \begin{bmatrix} q\tau_1(r_{11}E_1 + r_{12}E_2 + r_{13}E_3) & q\tau_1(r_{13}B_1 - r_{11}B_3) & q\tau_1(r_{11}B_2 - r_{12}B_1) \\ q\tau_2(r_{21}E_1 + r_{22}E_2 + r_{23}E_3) & 1 + q\tau_2(r_{23}B_1 - r_{21}B_3) & q\tau_2(r_{21}B_2 - r_{22}B_1) \\ q\tau_3(r_{31}E_1 + r_{32}E_2 + r_{33}E_3) & q\tau_3(r_{33}B_1 - r_{31}B_3) & 1 + q\tau_3(r_{31}B_2 - r_{32}B_1) \end{bmatrix}, \\
\overleftrightarrow{\Delta}_2 &= \begin{bmatrix} 1 + q\tau_1(r_{12}B_3 - r_{13}B_2) & q\tau_1(r_{11}E_1 + r_{12}E_2 + r_{13}E_3) & q\tau_1(r_{11}B_2 - r_{12}B_1) \\ q\tau_2(r_{22}B_3 - r_{23}B_2) & q\tau_2(r_{21}E_1 + r_{22}E_2 + r_{23}E_3) & q\tau_2(r_{21}B_2 - r_{22}B_1) \\ q\tau_3(r_{32}B_3 - r_{33}B_2) & q\tau_3(r_{31}E_1 + r_{32}E_2 + r_{33}E_3) & 1 + q\tau_3(r_{31}B_2 - r_{32}B_1) \end{bmatrix}, \\
\overleftrightarrow{\Delta}_3 &= \begin{bmatrix} 1 + q\tau_1(r_{12}B_3 - r_{13}B_2) & q\tau_1(r_{13}B_1 - r_{11}B_3) & q\tau_1(r_{11}E_1 + r_{12}E_2 + r_{13}E_3) \\ q\tau_2(r_{22}B_3 - r_{23}B_2) & 1 + q\tau_2(r_{23}B_1 - r_{21}B_3) & q\tau_2(r_{21}E_1 + r_{22}E_2 + r_{23}E_3) \\ q\tau_3(r_{32}B_3 - r_{33}B_2) & q\tau_3(r_{33}B_1 - r_{31}B_3) & q\tau_3(r_{31}E_1 + r_{32}E_2 + r_{33}E_3) \end{bmatrix}.
\end{aligned} \tag{D7}$$

By assuming $r_{ij} = 0$ for $i \neq j$, $r_{jj} = 1/m_j^*$ and introducing the notation $\mu_j = q\tau_j/m_j^*$, we find

$$\begin{aligned}
\overleftrightarrow{\mathcal{C}} &= \begin{bmatrix} 1 & -\mu_1 B_3 & \mu_1 B_2 \\ \mu_2 B_3 & 1 & -\mu_2 B_1 \\ -\mu_3 B_2 & \mu_3 B_1 & 1 \end{bmatrix}, \\
\overleftrightarrow{\Delta}_1 &= \begin{bmatrix} \mu_1 E_1 & -\mu_1 B_3 & \mu_1 B_2 \\ \mu_2 E_2 & 1 & -\mu_2 B_1 \\ \mu_3 E_3 & \mu_3 B_1 & 1 \end{bmatrix}, \\
\overleftrightarrow{\Delta}_2 &= \begin{bmatrix} 1 & \mu_1 E_1 & \mu_1 B_2 \\ \mu_2 B_3 & \mu_2 E_2 & -\mu_2 B_1 \\ -\mu_3 B_2 & \mu_3 E_3 & 1 \end{bmatrix}, \\
\overleftrightarrow{\Delta}_3 &= \begin{bmatrix} 1 & -\mu_1 B_3 & \mu_1 E_1 \\ \mu_2 B_3 & 1 & \mu_2 E_2 \\ -\mu_3 B_2 & \mu_3 B_1 & \mu_3 E_3 \end{bmatrix},
\end{aligned} \tag{D8}$$

and

$$\overleftrightarrow{\boldsymbol{\mu}}_c(\mathbf{B}) = -\frac{\mu_0}{1 + \mu_0^2 B^2} \begin{bmatrix} 1 + \mu_0^2 B_1^2 & -\mu_0 B_3 + \mu_0^2 B_1 B_2 & \mu_0 B_2 + \mu_0^2 B_1 B_3 \\ \mu_0 B_3 + \mu_0^2 B_2 B_1 & 1 + \mu_0^2 B_2^2 & -\mu_0 B_1 + \mu_0^2 B_2 B_3 \\ -\mu_0 B_2 + \mu_0^2 B_3 B_1 & \mu_0 B_1 + \mu_0^2 B_3 B_2 & 1 + \mu_0^2 B_3^2 \end{bmatrix}, \tag{D10}$$

where $B^2 = B_1^2 + B_2^2 + B_3^2$. By taking $\mathbf{B} = \{0, 0, B\}$, we find from Eq. (D10) that

$$\overleftrightarrow{\boldsymbol{\mu}}_c(\mathbf{B}) = -\frac{\mu_0}{1 + \mu_0^2 B^2} \begin{bmatrix} 1 & -\mu_0 B & 0 \\ \mu_0 B & 1 & 0 \\ 0 & 0 & 1 + \mu_0^2 B^2 \end{bmatrix}. \tag{D11}$$

386

For the surface case, $E_3 = 0$, $v_3 = 0$ and $\overleftrightarrow{\mathcal{M}}_s^{-1}$, $\overleftrightarrow{\boldsymbol{\tau}}_{sp}^{-1}$ and $\overleftrightarrow{\boldsymbol{\mu}}_s(\mathbf{B})$ for the $E_s^-(\mathbf{k}_{\parallel})$ (lower-cone) state all reduce to 2×2 tensors. This gives rise to

$$\begin{aligned}
\text{Det}\{\overleftrightarrow{\mathcal{C}}\} &= 1 + (B_1^2 \mu_2 \mu_3 + B_2^2 \mu_3 \mu_1 + B_3^2 \mu_1 \mu_2), \\
\text{Det}\{\overleftrightarrow{\Delta}_1\} &= \mu_1 E_1 + \mu_1 (B_3 E_2 \mu_2 - B_2 E_3 \mu_3) \\
&\quad + \mu_1 \mu_2 \mu_3 B_1 (\mathbf{E} \cdot \mathbf{B}), \\
\text{Det}\{\overleftrightarrow{\Delta}_2\} &= \mu_2 E_2 + \mu_2 (B_1 E_3 \mu_3 - B_3 E_1 \mu_1) \\
&\quad + \mu_1 \mu_2 \mu_3 B_2 (\mathbf{E} \cdot \mathbf{B}), \\
\text{Det}\{\overleftrightarrow{\Delta}_3\} &= \mu_3 E_3 + \mu_3 (B_2 E_1 \mu_1 - B_1 E_2 \mu_2) \\
&\quad + \mu_1 \mu_2 \mu_3 B_3 (\mathbf{E} \cdot \mathbf{B}).
\end{aligned} \tag{D9}$$

376

If we further assume $m_1^* = m_2^* = m_3^* = m_e^*$ and $\tau_1 = \tau_2 = \tau_3 = \tau_{pe}$, we obtain $\text{Det}\{\overleftrightarrow{\mathcal{C}}\} = 1 + \mu_0^2 B^2$, $\text{Det}\{\overleftrightarrow{\Delta}_1\} = -\mu_0 E_1 + \mu_0^2 (B_3 E_2 - B_2 E_3) - \mu_0^3 B_1 (\mathbf{E} \cdot \mathbf{B})$, $\text{Det}\{\overleftrightarrow{\Delta}_2\} = -\mu_0 E_2 + \mu_0^2 (B_1 E_3 - B_3 E_1) - \mu_0^3 B_2 (\mathbf{E} \cdot \mathbf{B})$, and $\text{Det}\{\overleftrightarrow{\Delta}_3\} = -\mu_0 E_3 + \mu_0^2 (B_2 E_1 - B_1 E_2) - \mu_0^3 B_3 (\mathbf{E} \cdot \mathbf{B})$, where $\mu_0 = e\tau_{pe}/m_e^*$. As a result, the mobility tensor $\overleftrightarrow{\boldsymbol{\mu}}_c(\mathbf{B})$, which is defined through $\mathbf{v}_d = \overleftrightarrow{\boldsymbol{\mu}}_c(\mathbf{B}) \cdot \mathbf{E}$, can be written as

377

378

379

380

381

382

383

$$\overleftrightarrow{\boldsymbol{\mu}}_s(\mathbf{B}) = \frac{\mu_1}{1 + \mu_1^2 B^2} \begin{bmatrix} 1 & \mu_1 B \\ -\mu_1 B & 1 \end{bmatrix}, \tag{D12}$$

where $\mu_1 = e\tau_{sp}v_F/(\hbar k_F^s)$, $k_F^s = \sqrt{4\pi\sigma_s}$ and σ_s is the areal density of surface electrons.

Appendix E: Bulk and surface conductivity tensors

Under a parallel external electric field $\mathbf{E} = (E_x, E_y, 0)$ and a perpendicular magnetic field $\mathbf{B} = (0, 0, B)$, the total parallel current per length in a p - n junction structure

is given by $\int_{-L_A}^{L_D} dz [\mathbf{j}_c^{\parallel}(z) + \mathbf{j}_v^{\parallel}(z)] + \mathbf{j}_s^{\pm}$, where L_D and L_A are the distribution ranges for donors and acceptors, respectively. Here, by using the second-order Boltzmann moment equation⁴², the bulk current densities are found to be

400

$$\mathbf{j}_{c,v}^{\parallel}(z) = \frac{2e\gamma_{e,h}m_{e,h}^*\tau_{e,h}(z)}{\tau_{p(e,h)}(z)} \mathbf{v}_{c,v}^{\parallel}[u_{c,v}(z)] \left\{ \left[\hat{\boldsymbol{\mu}}_{c,v}^{\parallel}(\mathbf{B}, z) \cdot \mathbf{E} \right] \right\} \cdot \mathbf{v}_{c,v}^{\parallel}[u_{c,v}(z)] \mathcal{D}_{c,v}[u_{c,v}(z)] , \quad (\text{E1})$$

401 where $\mathcal{D}_{c,v}[u_{c,v}(z)] = (\sqrt{u_{c,v}(z)}/4\pi^2) (2m_{e,h}^*/\hbar^2)^{3/2}$ is
 402 the electron and hole density-of-states per spin, $u_{c,v}(z) =$
 403 $(\hbar k_F^{e,h})^2/2m_{e,h}^*$ and $k_F^{e,h}$ are Fermi energies and wave vec-
 404 tors in a bulk, $m_{e,h}^*$ are effective masses of electrons and
 405 holes, $\tau_{e,h}(z)$ and $\tau_{p(e,h)}(z)$ are bulk energy- and momen-
 406 tum relaxation times,^{37,40,41} $\mathbf{v}_{c,v}^{\parallel}(\mathbf{k}) = -\gamma_{e,h} \hbar \mathbf{k}_{\parallel}/m_{e,h}^*$,
 407 and $\gamma_{e,h} = -1$ (electrons) and $+1$ (holes), respectively.
 408 Similarly, the surface current per length is⁴²

$$\mathbf{j}_s^{\pm} = \mp \frac{e\tau_s \hbar k_F^s}{\tau_{sp} v_F} \mathbf{v}_s^{\pm}(u_s) \left\{ \left[\hat{\boldsymbol{\mu}}_s^{\pm}(\mathbf{B}) \cdot \mathbf{E} \right] \right\} \cdot \mathbf{v}_s^{\pm}(u_s) \rho_s(u_s) , \quad (\text{E2})$$

409 where $\rho_s(u_s) = u_s/(2\pi\hbar^2 v_F^2)$ and $u_s = \hbar v_F k_F^s$ are the
 410 surface density-of-states and Fermi energy, $k_F^s = \sqrt{4\pi\sigma_s}$,
 411 v_F is the Fermi velocity of a Dirac cone, τ_s and τ_{sp} are
 412 surface energy- and momentum relaxation times,^{37,40,41}

and $\mathbf{v}_s^{\pm}(\mathbf{k}_{\parallel}) = \pm(\mathbf{k}_{\parallel}/k_{\parallel}) v_F$.

413 From Eq. (E1), we find the bulk conductivity tensor as

$$\hat{\boldsymbol{\sigma}}_{c,v}^{\parallel}(\mathbf{B}) = e\gamma_{e,h} \int_{-L_A}^{L_D} dz n_{e,h}(z) \left[\frac{\tau_{e,h}(z)}{\tau_{p(e,h)}(z)} \right] \hat{\boldsymbol{\mu}}_{c,v}^{\parallel}(\mathbf{B}, z) . \quad (\text{E3})$$

415 On the other hand, from Eq. (E2) we get the surface
 416 conductivity tensor, given by

$$\hat{\boldsymbol{\sigma}}_s^{\pm}(\mathbf{B}) = e\sigma_s \left(\frac{\tau_s}{\tau_{sp}} \right) \hat{\boldsymbol{\mu}}_s^{\pm}(\mathbf{B}) . \quad (\text{E4})$$

417 Therefore, the total conductivity tensor $\hat{\boldsymbol{\sigma}}_{tot}(\mathbf{B}) =$
 418 $\hat{\boldsymbol{\sigma}}_c^{\parallel}(\mathbf{B}) + \hat{\boldsymbol{\sigma}}_v^{\parallel}(\mathbf{B}) + \hat{\boldsymbol{\sigma}}_s^{\pm}(\mathbf{B})$ can be obtained from

$$\begin{aligned} \hat{\boldsymbol{\sigma}}_{tot}(\mathbf{B}) = & e \hat{\boldsymbol{\mu}}_v^{\parallel}(\mathbf{B}) N_A A_h \left[(L_A - W_p) + \int_0^{W_p} dz \exp\left(-\frac{\beta e \bar{\mu}_h N_A}{2\epsilon_0 \epsilon_r D_h} z^2\right) \right] \\ & - e \hat{\boldsymbol{\mu}}_c^{\parallel}(\mathbf{B}) N_D A_e \left[(L_D - W_n) + \int_0^{W_n} dz \exp\left(-\frac{\beta e \bar{\mu}_e N_D}{2\epsilon_0 \epsilon_r D_e} z^2\right) \right] + e \hat{\boldsymbol{\mu}}_s^{\pm}(\mathbf{B}) \left(\frac{\alpha_0^2}{4\pi\hbar^2 v_F^2} \right) (L_A - L_0)^2 A_s , \quad (\text{E5}) \end{aligned}$$

419 where α_0 and L_0 are constants to be determined exper-
 420 imentally, $N_{D,A}$ are doping concentrations, W_n and W_p
 421 are depletion ranges for donors and acceptors in a p - n
 422 junction, $\bar{\mu}_{e,h}$ are $\mu_0(z)$ evaluated at $n_{e,h}(z) = N_{D,A}$,
 423 $D_{e,h}$ are diffusion coefficients, and $\beta = 4/3$ ($\beta = 7/3$)
 424 for longitudinal (Hall) conductivity. In addition, the av-
 425 eraged mobilities $\hat{\boldsymbol{\mu}}_{c,v}^{\parallel}(\mathbf{B})$ are defined by their values of
 426 $\tau_{p(e,h)}(z)$ at $n_{e,h}(z) = N_{D,A}$, and three introduced coef-
 427 ficients are $A_s = \tau_s/\tau_{sp} \approx 3/4$,

$$\begin{aligned} A_{e,h} = & \frac{\tau_{e,h}(z)}{\tau_{p(e,h)}(z)} \Big|_{n_{e,h}(z)=N_{D,A}} \\ = & \frac{1}{6} \left(\frac{Q_c}{k_F^{e,h}} \right)^2 \left[2 \ln \left(\frac{2k_F^{e,h}}{Q_c} \right) - 1 \right] \\ = & \frac{Q_c^2}{6(3\pi^2 N_{D,A})^{2/3}} \left\{ 2 \ln \left[\frac{2(3\pi^2 N_{D,A})^{1/3}}{Q_c} \right] - 1 \right\} , \quad (\text{E6}) \end{aligned}$$

where $1/Q_c$ is the Thomas-Fermi screening length.

428 In addition, the bulk energy-relaxation times $\tau_{e,h}(z)$
 429 are calculated as^{37,40,41}

$$\begin{aligned} \frac{1}{\tau_{e,h}(z)} = & \left[\frac{2n_i}{n_{e,h}(z)\pi\hbar Q_c^2} \right] \left(\frac{e^2}{\epsilon_0 \epsilon_r} \right)^2 \times \\ & \int_0^{k_F^{e,h}(z)} dk \mathcal{D}_{c,v}(\epsilon_k^{c,v}) \left(\frac{4k^2}{4k^2 + Q_c^2} \right) \\ = & \left[\frac{n_i m_{e,h}^*}{8n_{e,h}(z)\pi^3 \hbar^3 Q_c^2} \right] \left(\frac{e^2}{\epsilon_0 \epsilon_r} \right)^2 \times \\ & \left\{ [2k_F^{e,h}(z)]^2 - Q_c^2 \ln \left(\frac{[2k_F^{e,h}(z)]^2 + Q_c^2}{Q_c^2} \right) \right\} , \quad (\text{E7}) \end{aligned}$$

431 and the surface energy-relaxation time τ_s is found to
 432 be^{37,40,41}

$$\frac{1}{\tau_s} = \frac{2\sigma_i}{\pi^2 \sigma_s \hbar^2 v_F} \left(\frac{e^2}{2\epsilon_0 \epsilon_r} \right)^2 \times \int_0^{\pi} d\phi \int_0^{k_F^s} \frac{k_{\parallel}^2 dk_{\parallel}}{(q_c + 2k_{\parallel} |\cos \phi|)^2} , \quad (\text{E8})$$

433 where n_i and σ_i are the impurity concentration and sur-

face density, respectively.

434
435 Finally, the bulk chemical potentials for electrons
436 $[u_c(z)]$ and holes $[u_v(z)]$ are calculated as

$$[u_{c,v}(z)]^{3/2} = 3\pi^2 \left(\frac{\hbar^2}{2m_{e,h}^*} \right)^{3/2} n_{e,h}(z), \quad (\text{E9})$$

437 and the carrier density functions are

$$n_{e,h}(z) = N_{D,A} \times \exp \left\{ -\gamma_{e,h} \left(\frac{\bar{\mu}_{e,h}}{D_{e,h}} \right) \left[\Phi(z) + \gamma_{e,h} (E_F^{e,h}/e) \right] \right\}. \quad (\text{E10})$$

438 Here, the expression for the introduced potential function

439 $\Phi(z)$ is given by

$$\Phi(z) = \begin{cases} -E_F^h/e, & z < -W_p \\ -E_F^h/e + (eN_A/2\epsilon_0\epsilon_r)(z + W_p)^2, & -W_p < z < 0 \\ E_F^e/e - (eN_D/2\epsilon_0\epsilon_r)(W_n - z)^2, & 0 < z < W_n \\ E_F^e/e, & z > W_n \end{cases}, \quad (\text{E11})$$

440 and E_F^e (E_F^h) is the Fermi energy of electrons (holes) at
441 zero temperature and defined far away from the depletion
442 region.

443 * db639@cam.ac.uk

444 † vn237@cam.ac.uk

445 ¹ M. Z. Hasan and C. L. Kane, Rev. Mod. Phys. **82**, 3045
446 (2010).

447 ² D. Hsieh, Y. Xia, L. Wray, D. Qian, A. Pal, J. H. Dil,
448 J. Osterwalder, F. Meier, G. Bihlmayer, C. L. Kane, Y.
449 S. Hor, R. J. Cava, and M. Z. Hasan, Science **323**, 919
450 (2009).

451 ³ Y. Xia, D. Qian, D. Hsieh, L. Wray, A. Pal, H. Lin, A.
452 Bansil, D. Grauer, Y. S. Hor, R. J. Cava, and M. Z. Hasan,
453 Nat. Phys. **5**, 18 (2009).

454 ⁴ Y. L. Chen, J. G. Analytis, J.-H. Chu, Z. K. Liu, S.-K. Mo,
455 X. L. Qi, H. J. Zhang, D. H. Lu, X. Dai, Z. Fang, S. C.
456 Zhang, I. R. Fisher, Z. Hussain, and Z.-X. Shen, Science
457 **325**, 178 (2009).

458 ⁵ D. Hsieh, D. Qian, L. Wray, Y. Xia, Y. S. Hor, R. J. Cava,
459 and M. Z. Hasan, Nature **452**, 970 (2008).

460 ⁶ J. Chen, H. J. Qin, F. Yang, J. Liu, T. Guan, F. M. Qu,
461 G. H. Zhang, J. R. Shi, X. C. Xie, C. L. Yang, K. H. Wu,
462 Y. Q. Li, and L. Lu, Phys. Rev. Lett. **105**, 176602 (2010).

463 ⁷ J. Chen, X. Y. He, K. H. Wu, Z. Q. Ji, L. Lu, J. R. Shi, J.
464 H. Smet, and Y. Q. Li, Phys. Rev. B **83**, 241304 (2011).

465 ⁸ J. G. Checkelsky, Y. S. Hor, R. J. Cava, and N. P. Ong,
466 Phys. Rev. Lett. **106**, 196801 (2011).

467 ⁹ H. Steinberg, J. B. Laloe, V. Fatemi, J. S. Moodera, and
468 P. Jarillo-Herrero, Phys. Rev. B **84**, 233101 (2011).

469 ¹⁰ D. Kong, Y. Chen, J. J. Cha, Q. Zhang, J. G. Analytis, K.
470 Lai, Z. Liu, S. S. Hong, K. J. Koski, S.-K. Mo, Z. Hussain,
471 I. R. Fisher, Z.-X. Shen, and Y. Cui, Nat. Nanotechnol. **6**,
472 705 (2011).

473 ¹¹ J. Zhang, C.-Z. Chang, Z. Zhang, J. Wen, X. Feng, K. Li,
474 M. Liu, K. He, L. Wang, X. Chen, Q.-K. Xue, X. Ma, and
475 Y. Wang, Nat. Commun. **2**, 574 (2011).

476 ¹² C. Weyrich, M. Drögeler, J. Kampmeier, M. Eschbach, G.
477 Mussler, T. Merzenich, T. Stoica, I. E. Batov, J. Schubert,
478 L. Plucinski, B. Beschoten, C. M. Schneider, C. Stampfer,
479 D. Grützmacher, Th. Schäpers, J. Phys.: Condens. Matter
480 **28**, 495501 (2016).

481 ¹³ Z. Zhang, X. Feng, M. Guo, Y. Ou, J. Zhang, K. Li, L.
482 Wang, X. Chen, Q. Xue, X. Ma, K. He, and Y. Wang,
483 Phys. Status Solidi RRL **7**, 142 (2013).

484 ¹⁴ M. Eschbach, E. Mlynczak, J. Kellner, J. Kampmeier, M.

485 Lanius, E. Neumann, C. Weyrich, M. Gehlmann, P. Gospo-
486 daric, S. Döring, G. Mussler, N. Demarina, M. Luysberg,
487 G. Bihlmayer, T. Schapers, L. Plucinski, S. Blügel, M.
488 Morgenstern, C. M. Schneider, and D. Grützmacher, Nat.
489 Commun. **6**, 8816 (2015).

490 ¹⁵ M. Lanius, J. Kampmeier, C. Weyrich, S. Kölling, M.
491 Schall, P. Schuelgen, E. Neumann, M. Luysberg, G. Mus-
492 sler, P. M. Koenraad, T. Schaeppers, and D. Grützmacher,
493 Cryst. Growth Des. **16**, 2057 (2016).

494 ¹⁶ O. Klein, Z. Phys. **53**, 157 (1929).

495 ¹⁷ M. Katsnelson, K. Novoselov, and A. Geim, Nat. Phys. **2**,
496 620 (2006).

497 ¹⁸ R. Ilan, F. de Juan, and J. E. Moore, Phys. Rev. Lett.
498 **115**, 096802 (2015).

499 ¹⁹ B. Seradjeh, J. E. Moore, and M. Franz, Phys. Rev. Lett.
500 **103**, 066402 (2009).

501 ²⁰ D.-X. Qu, Y. Hor, J. Xiong, R. Cava, and N. Ong, Science
502 **329**, 821 (2010).

503 ²¹ X. Wang, Y. Du, S. Dou, and C. Zhang, Phys. Rev. Lett.
504 **108**, 266806 (2012).

505 ²² T. Liang, Q. Gibson, M. Ali, M. Liu, R. Cava, and N. Ong,
506 Nat. Mater. **14**, 280 (2015).

507 ²³ A. A. Abrikosov, Phys. Rev. B **58**, 2788 (1998).

508 ²⁴ M. M. Parish and P. B. Littlewood, Nature **426**, 162
509 (2003).

510 ²⁵ A. Narayanan, M. D. Watson, S. F. Blake, N. Bruyant, L.
511 Drigo, Y. L. Chen, D. Prabhakaran, B. Yan, C. Felser, T.
512 Kong, P. C. Canfield, and A. I. Coldea, Phys. Rev. Lett.
513 **114**, 117201 (2015).

514 ²⁶ S. Hikami, A. I. Larkin, and Y. Nagaoka, Prog. Theor.
515 Phys. **63**, 707 (1980).

516 ²⁷ B. L. Altshuler, A. G. Aronov, and D. E. Khmel'nitsky, J
517 Phys. C: Sol. State Phys. **15**, 7367 (1998).

518 ²⁸ Y. Takagaki, A. Giussani, K. Perumal, R. Calarco, and K.
519 J. Friedland, Phys. Rev. B **86**, 125137 (2012).

520 ²⁹ T.-A. Nguyen, D. Backes, A. Singh, R. Mansell, C. Barnes,
521 D. A. Ritchie, G. Mussler, M. Lanius, D. Grützmacher, and
522 V. Narayan, Sci. Rep. **6**, 27716 (2016).

523 ³⁰ I. Garate and L. Glazman, Phys. Rev. B **86**, 035422 (2012).

524 ³¹ M. Veldhorst, M. Snelder, M. Hoek, C. G. Molenaar, D. P.
525 Leusink, A. A. Golubov, H. Hilgenkamp, and A. Brinkman,
526 Phys. Status Solidi RRL **7**, 26 (2013).

- 527 ³² G. Schubert, H. Fehske, L. Fritz, and M. Vojta, Phys. Rev. 539
528 B **85**(R) 201105 (2012). 540
- 529 ³³ C. Kittel, Introduction to Solid State Physics, 6th ed. 541
530 (John Wiley & Sons, Inc., New York, 1986). 542
- 531 ³⁴ Z. Ren, A. A. Taskin, S. Sasaki, K. Segawa, and Y. Ando, 543
532 Phys. Rev. B **82**, 241306 (R) (2010). 544
- 533 ³⁵ G. Eguchi and S. Paschen, arXiv: 1609.04134. 545
- 534 ³⁶ J. Horak, C. Drasar, R. Novotny, S. Karamazov, and P. 546
535 Lostak, Phys. Status Solidi A **149**, 549 (1995). 547
- 536 ³⁷ D. Huang, T. Apostolova, P. M. Alsing, and D. A. Cardi- 548
537 mona, Phys. Rev. B **69**, 075214 (2004). 549
- 538 ³⁸ V. Narayan, T.-A. Nguyen, R. Mansell, D. Ritchie, and G. 550
551 Mussler, Phys. Status Solidi RRL **10**, 253 (2016).
- ³⁹ I. Belopolski, S.-Y. Xu, N. Koirala, C. Liu, G. Bian, V. N. 540
Strocov, G. Chang, M. Neupane, N. Alidoust, D. Sanchez, 541
H. Zheng, M. Brahlek, V. Rogalev, T. Kim, N. C. Plumb, 542
C. Chen, F. Bertran, P. Le Fèvre, A. Taleb-Ibrahimi, M.- 543
C. Asensio, M. Shi, H. Lin, M. Hoesch, S. Oh and M. Z. 544
Hasan, Sci. Adv. **3**, 1501692 (2017). 545
- ⁴⁰ D. H. Haung and G. Gumbs, Phys. Rev. B **80**, 033411 546
(2009). 547
- ⁴¹ D. H. Huang, P. M. Alsing, T. Apostolova, and D. A. 548
Cardimona, Phys. Rev. B **71**, 195205 (2005). 549
- ⁴² D. H. Haung, G. Gumbs and O. Roslyak, J. Mod. Opt. **58**, 550
1898 (2011). 551